Comments on Inorganic Chemistry
Publication details, including instructions for authors and subscription information:
http://www.informaworld.com/smpp/title~content=t713455155

Ligand-Field Splittings on Core Levels of Main Group Compounds and Metal Surfaces from Photoelectron Spectra

G. M. Bancroft[a]; J. S. Tse[b]
[a] Department of Chemistry, Centre for Chemical Physics, University of Western Ontario, London, Ontario, Canada [b] Chemistry Division, National Research Council, Ottawa, Ontario, Canada

To cite this Article Bancroft, G. M. and Tse, J. S.(1986) 'Ligand-Field Splittings on Core Levels of Main Group Compounds and Metal Surfaces from Photoelectron Spectra', Comments on Inorganic Chemistry, 5: 2, 89 — 118
To link to this Article: DOI: 10.1080/02603598608072277
URL: http://dx.doi.org/10.1080/02603598608072277

Ligand-Field Splittings on Core Levels of Main Group Compounds and Metal Surfaces from Photoelectron Spectra

In the last 10 years, ligand-field splittings on core levels of main group compounds (e.g., compounds of Zn, Cd, In, Tl, Xe, I) in the gas phase have been observed using high resolution photoelectron spectroscopy. These splittings on d^9 and p^5 ion states are analogous to the well-known splittings of valence d levels in transition metals, and are characterized using the usual crystal-field and spin-orbit Hamiltonian. The noncubic C_2^0 term dominates these splittings. The C_2^0 values are sensitive to structure and bonding. For example, C_2^0 increase for R_2Zn compounds in the order R = Cl < Br < I < Me < Et—just the order of increasing σ donor strength, and the In 4d splitting has been useful in showing that indium trihalides are dimers in the gas phase. Simple calculations are useful for calculating these splittings, especially point charge calculations for the I splittings in alkali iodides. The C_2^0 Hamiltonian term transforms like the nuclear quadrupole Hamiltonian, making it possible to observe the transmission of the ligand field through the atom to the nucleus. Monochromatized synchrotron radiation as a photoelectron source will be important for observing these splittings in more gas phase compounds of a variety of elements, and also for examining core level broadenings on surfaces.

INTRODUCTION

The splitting of partially filled metal-valence d orbitals in transition metal complexes has been the subject of intense study in the last few decades. The theoretical framework for these splittings was initiated with the crystal-field theory of Becquerel[1] and Bethe.[2] These papers showed how the symmetry and strength of the electric field from the ligands could affect the electronic levels of gaseous metal ions. With the advent of spectrophotometers, hundreds of

Comments Inorg. Chem.
1986, Vol. 5, No. 2, pp. 89–118
0260-3594/86/0502-0089/$25.00/0

electronic spectra of transition metal compounds were measured and interpreted[3] using crystal-field theory and/or ligand-field theory.[4-6] This research has been extremely important, not only for understanding the many interesting ligand–d electron interactions, but also for characterizing geometries of metal complexes and the bonding properties of ligands. This spectroscopic work played an important role in the rapid development of inorganic chemistry in the 1950s and 1960s.

Recently, ligand-field splittings of similar origin have been observed and characterized[7-12] on core level d^9 and p^5 ion states of main group compounds in the gas phase using photoelectron spectroscopy. This splitting has been, and will be, important for characterizing bonding and structure in volatile compounds of main group elements, and surfaces of main group and transition metal semiconductor and metal surfaces. The theoretical framework for this splitting is based on the crystal-field Hamiltonian used widely to interpret the transition metal d splittings.[4,6]

In this Comment, we begin by examining crystal-field theory as applied to d^1 and d^9 transition metal ion spectra. We then show how this same theory is applied to the main group element d^9 and p^5 ion states. We show that the splitting is sensitive to the molecular symmetry and bonding properties of ligands, and examine the known photoelectron data. The relationship of this ligand-field splitting to the electric field gradient at the nucleus is then examined. Finally, we speculate on forthcoming experimental and theoretical developments.

CRYSTAL-FIELD THEORY OF TRANSITION METAL IONS

As background to the ligand-field splitting of main group elements discussed in this Comment, it is worthwhile to review simple crystal-field concepts using d^1 and d^9 transition metal ions. Consider the simplest example of Ti^{3+} having one 3d electron in the octahedral complex $Ti(H_2O)_6^{3+}$. The free ion yields a ^2D term ($L = 2$ and $2S + 1 = 2$). In the complex, the ^2D term splits into two levels, the ^2E_g and ^2T_g states (Fig. 1(A)) by the interaction of the octahedral field with the one d electron. The transition from $T_{2g} \rightarrow E_g$

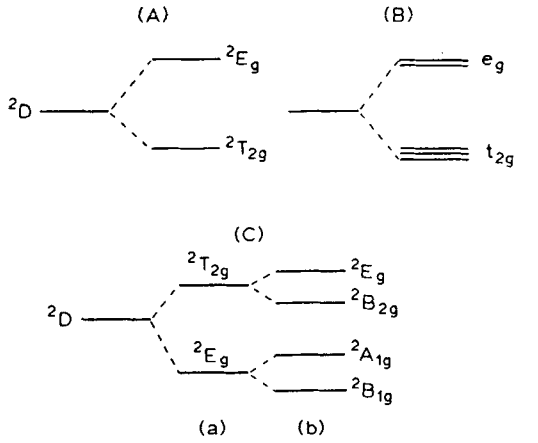

FIGURE 1 Energy-level diagrams for the splitting of d orbitals in crystal fields: (A) Octahedral splitting of a ^2D term from a Ti^{3+} ion ($3d^1$) into ^2E_g and $^2T_{2g}$ states. (B) Splitting of d orbitals into $e_g(d_{z^2}$ and $d_{x^2-y^2})$ and $t_{2g}(d_{xy}$, d_{xz}, $d_{yz})$ subsets. (C) Splitting of the ^2D term in a Cu^{2+} ion by (a) an octahedral field and (b) by a tetragonal field.

results in an absorption band at 20,300 cm^{-1} in the $Ti(H_2O)_6^{3+}$ complex.[5,6] In one-electron terms, the $^2T_{2g} \rightarrow {}^2E_g$ transition corresponds to a one-electron transition from a $t_{2g}(d_{xz}$, d_{yz} or $d_{xy})$ orbital to an $e_g(d_{x^2-y^2}$ or $d_{z^2})$ orbital (Fig. 1(B)).

A somewhat analogous picture develops for a $Cu^{2+}(3d^9)$ ion. According to the hole–particle analogy,[4-6] the spectral behavior of an octahedral $Cu(H_2O)_6^{2+}$ complex should be as found in $Ti(H_2O)_6^{3+}$, only with the order of states inverted (Fig. 1(C)). The ground state now is a ^2E_g state. The one-electron picture for the $3d^9$ configuration remains the same as that for d^1 with the t_{2g} d electrons being at low energy (Fig. 1(B)). A tetragonal distortion in Cu^{2+} complexes results in a further splitting of both the T_{2g} and E_g levels (Fig. 1(C)).

One more Cu^{2+} example is important—the splitting of the d orbitals in the linear $CuCl_2$ complex in the gas phase.[13] In this linear molecule, two absorption bands are seen at 9000 cm^{-1} and 18,000 cm^{-1}, and the resulting energy level diagram is seen in Fig. 2. The term symbols for a $D_{\infty h}$ or $C_{\infty v}$ molecule are Σ, Π and Δ, and the order of these states is $\Delta > \Pi > \Sigma$. This corresponds to the opposite one-electron order $\sigma(d_z^2) > \pi(d_{xz},d_{yz}) > \delta(d_{xy},d_{x^2-y^2})$.

Of course, the Cl^- ligands pointing towards d_{z^2} will destabilize it the most of the d orbitals, and d_{z^2} is at highest energy.

For the linear $CuCl_2$ molecule, the required crystal-field potential is[13]:

$$V = A_0^0 Y_0^0 + A_2^0 r^2 Y_2^0 + A_4^0 r^4 Y_4^0 \tag{1}$$

where the A are expansion coefficients for the spherical harmonics Y_l^m.

The $A_0^0 Y_0^0$ term has no angular dependence and just shifts all d orbitals by the same amount. The A_2^0 and A_4^0 terms give rise to the splitting in Fig. 2. The methods of operator equivalents[14] is conveniently used for calculation of the matrix elements of V, and H becomes (neglecting the $A_0^0 Y_0^0$ term):

$$H = C_2^0[3L_z^2 - L(L+1)] + C_4^0[35L_z^4 - 30L(L+1)L_z^2 + 25L_z^2 - 6L(L+1) + 3L^2(L+1)^2] \tag{2}$$

Considering just the C_2^0 term in the Hamiltonian ($H_{C_2^0}$), the energy levels can be obtained easily for $M_L = \pm 2(d_{xy}, d_{x^2-y^2})$, $\pm 1(d_{xz}, d_{yz})$ and $0(d_{z^2})$ for the d^1 case. Thus, $\langle 2|H_{C_2^0}|2\rangle = 6C_2^0$, $\langle 1|H_{C_2^0}|1\rangle = -3C_2^0$, and $\langle 0|H_{C_2^0}|0\rangle = -6C_2^0$. The diagonal elements for the C_4^0 term are obtained similarly. Using the hole–particle analogy,

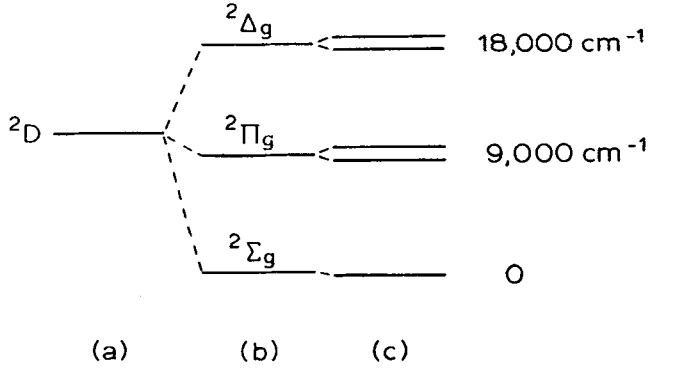

FIGURE 2 Energy levels of Cu^{2+} in: (a) free ion; (b) linear $CuCl_2$ in the gas phase; and (c) with spin-orbit splitting included (Ref. 13).

the signs for Cu^{2+} (d^9) are reversed, and the energy levels are obtained:

$$E_\Sigma = +6C_2^0 + 72C_4^0 \tag{3a}$$

$$E_\Pi = +3C_2^0 - 48C_4^0 \tag{3b}$$

$$E_\Delta = -6C_2^0 + 12C_4^0 \tag{3c}$$

These are just the expressions obtained by Hougen *et al.* using A_2 and A_4 parameters[13] taking $C_2^0 = 2/3\ A_2$ and $C_4^0 = 1/6\ A_4$. From the two observed UV transitions at 9,000 cm^{-1} and 18,000 cm^{-1}, and knowing from the above electrostatic arguments that $E_\Delta > E_\Pi > E_\Sigma$, we can readily solve for $C_4^0 = -43\ cm^{-1}$ (0.005 eV) and $C_2^0 = -1286\ cm^{-1}$ (0.159 eV). Notice that both signs are negative and that $C_2^0/C_4^0 \simeq 30$.

Spin-orbit splitting further splits the $^2\Pi$ and $^2\Delta$ states (Fig. 2) and the Hamiltonian for this interaction is given by:

$$H_{S.O.} = \lambda[(1/2)(L_-S_+ + L_-S_+) + L_zS_z] \tag{4}$$

Five energy levels result. λ_{3d} for the free Cu^{2+} ion is 830 cm^{-1},[15] so this splitting is much smaller than that due to the ligand field from the Cl^- ions. We will see shortly that an exactly analogous treatment to the one given here is appropriate for the interpretation of the main group ligand-field splittings.

CORE-LEVEL PHOTOELECTRON SPECTROSCOPY

Photoelectron spectroscopy has been divided into two distinct areas because of the availability of simple intense light sources. If the photon energy is in the vacuum ultraviolet (VUV) range [for example, HeI (21.1 eV) or HeII (40.8 eV)], the technique is often called ultraviolet photoelectron spectroscopy (UPS).[16,17] If the photon energy is in the x-ray range [for example, Al $K\alpha$ (1486 eV)], the technique is called x-ray photoelectron spectroscopy (XPS or ESCA).[16,18] The former technique has been used predominantly to study valence levels of gases at high instrumental resolution

($\leq$ 20 meV or 160 cm^{-1}) and solids at lower resolution ($\leq$0.3 eV), while the latter technique is used normally to study core levels at comparatively low resolution (~1 eV). The distinction between these two fields is becoming blurred by the use of synchrotron radiation[19,20,21] which can provide good resolution at photon energies $\gg$ 40 eV.

In photoelectron spectroscopy, photons of energy $h\nu$ interact with electrons in a molecule, and the electrons are ejected with kinetic energies (E_k) given by the Einstein formula:

$$h\nu = E_b + E_k \tag{5}$$

where E_b is the electron binding energy. The kinetic energies E_k are measured with an electrostatic or magnetic analyzer: $h\nu$ is known, so that the binding energies can be readily obtained. A photoelectron spectrum consists of a plot of number of photoelectrons detected versus E_k (or E_b). Fig. 3 shows that at least one peak is obtained for each atomic and molecular orbital in a mol-

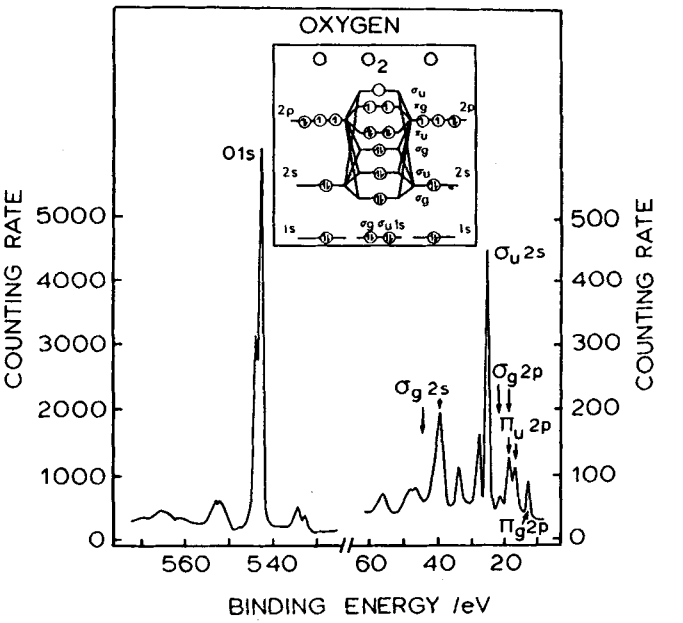

FIGURE 3 The x-ray photoelectron spectrum of O_2 from Ref. 18.

ecule such as O_2.[18] The binding energies can be directly related to one-electron molecular orbital energies by Koopman's theorem[22] which states that the negative of the one-electron eigenvalue is equal to its binding energy. This assumes that all other electrons remain frozen during the photoionization process.

There are a number of interesting effects in core-level spectroscopy which have received much chemical attention: chemical shifts, shakeup satellites, multiplet splitting and spin-orbit splitting.[16-18] Spin-orbit splitting is always observed in p, d and f core-level spectra, and this is best described considering the ion state after ejection of the electron. For example, in the case of an atom such as Ar with filled $2p^6$ and $3p^6$ shells, photoionization of a 2p or 3p electron yields a p^5 ion. Coupling of the hole spin with the orbital angular momentum gives rise to $^2P_{3/2}$ and $^2P_{1/2}$ states (Fig. 4). The x-ray spectrum of the Ar 2p level and the UV spectrum of the Ar 2p level (Fig. 5) illustrate two important points. First, the linewidths of two 3p spin-orbit peaks are $\leq$ 20 meV (Fig. 5(b)) while the linewidths of the two 2p spin-orbit peaks are $\geq$ 0.9 eV (Fig. 5(a)). Second, the spin-orbit splitting increases greatly going from the valence Ar 3p level to the core Ar 2p electrons.

Similarly, an ionized core d^{10} shell gives a $^2D_{5/2}$ and $^2D_{3/2}$ spin-orbit doublet, and an ionized core f^{14} shell gives an $^2F_{7/2}$ and $^2F_{5/2}$ spin-orbit doublet. The photoionization process creates a p^5, d^9 or f^{13} ion, and 12 years ago it seemed reasonable to us that the electric field produced by the ligands would split the ^2D states in an analogous way to the splitting of the ^2D state in Cu^{2+} (Fig. 2) and five peaks in the photoelectron spectrum would

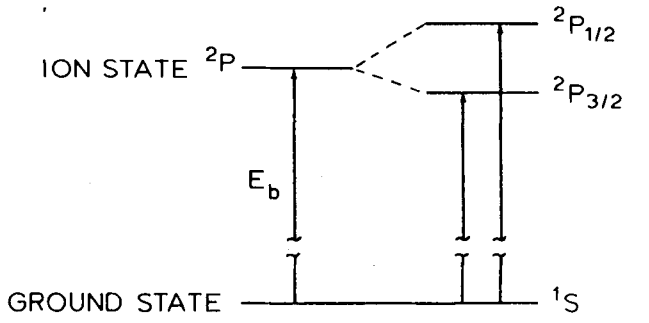

FIGURE 4 Energy-level diagram for the transitions observed in a photoelectron spectrum after ejection of a p electron.

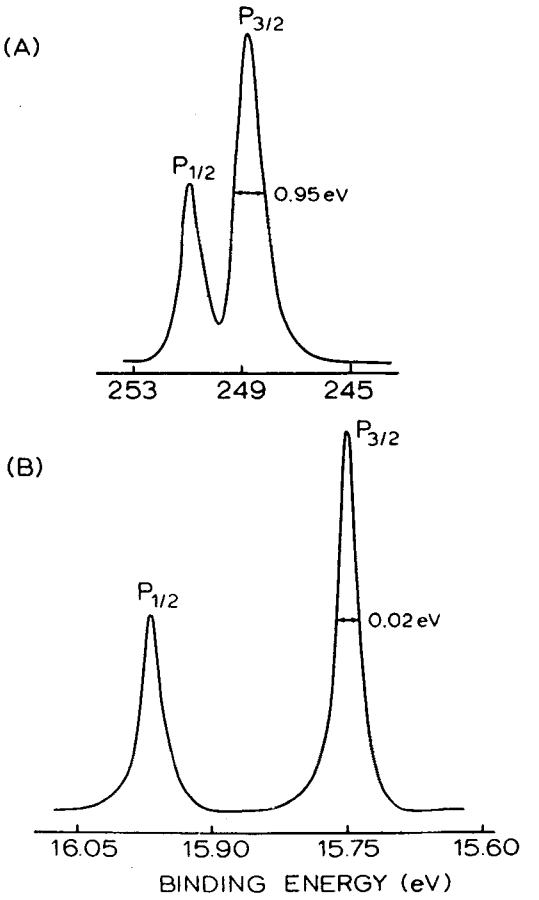

FIGURE 5 Photoelectron spectra of the p electrons in Ar: (a) Ar 2p spectrum taken with Mg $K\alpha$ radiation; (b) Ar 3p spectrum taken with HeI radiation. Notice the difference in binding energy scales and linewidths in the two spectra.

result. The relative magnitudes of the spin-orbit and ligand-field effects would be different of course for core orbitals.

LIGAND-FIELD SPLITTING ON CORE d LEVELS

Theoretical[23,24] and experimental results[25,26,27] up to 1975 gave us confidence that core d orbitals did indeed split due to ligand-field

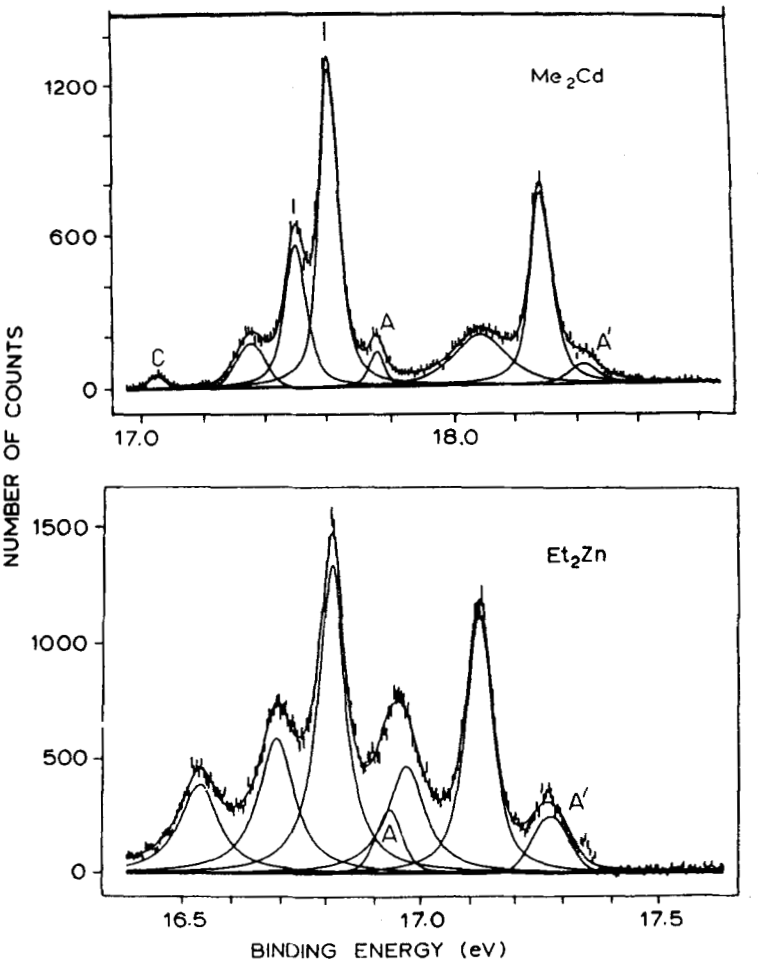

FIGURE 6 Photoelectron spectra of the Cd 4d levels in Me_2Cd and Zn 3d levels in Et_2Zn taken with HeII radiation (40.8 eV) (Ref. 8). Peaks A and A′ are thought to be due to RM radicals and peak C is due to the He^+ peak excited by 48.4 eV radiation (HeIIβ).

splitting. More than two peaks (but less than five) were observed in the Zn 3d levels in Me_2Zn[26] and the Zn halides,[27] but the effect was not fully characterized because five lines were not resolved.

The Me_2Cd Cd 4d spectrum reported in 1976[28] showed five clearly resolved lines, and this gave us the opportunity of characterizing the ligand-field splitting fully. Two high-resolution spec-

tra of Me_2Cd and Et_2Zn taken with HeII radiation are shown in Fig. 6.[8,29] Apart from some small impurity peaks (labelled A, A′, and C), the spectra consist of five peaks—a $D_{5/2}$ triplet and a $D_{3/2}$ doublet. Combining the crystal-field Hamiltonian for this linear molecule (Eq. (2)) with the spin-orbit interaction (Eq. (4)), it is still relatively easy to diagonalize the Hamiltonian matrix. The resulting equations for the five energies are (with the approximate term symbols)[7]:

$$E(^2\Delta_{5/2}) = E_{4d} - 6C_2^0 + 12C_4^0 - \lambda, \tag{6a}$$

$$E(^2\Delta_{3/2}) = E_{4d} - 3/2C_2^0 - 18C_4^0 + 1/4\,\lambda + \frac{1}{2}\sqrt{\begin{array}{l} 81C_4^{02} - 1080C_2^0C_4^0 - 27C_2^0\lambda \\ + 3600C_4^{02} + 180C_4^0\lambda + \frac{25}{4}\lambda^2 \end{array}}, \tag{6b}$$

$$E(^2\Pi_{3/2}) = E_{4d} - 3/2\,C_2^0 - 18C_4^0 + 1/4\,\lambda - \frac{1}{2}\sqrt{\begin{array}{l} 81C_2^{02} - 1080C_2^0C_4^0 - 27C_2^0\lambda \\ + 3600C_4^{02} + 180C_4^0\lambda + \frac{25}{4}\lambda^2, \end{array}} \tag{6c}$$

$$E(^2\Pi_{1/2}) = E_{4d} + 9/2C_2^0 + 12C_4^{02} + 1/4\,\lambda + \frac{1}{2}\sqrt{\begin{array}{l} 9C^{02} + 72C_2^0C_4^0 - 3C_2^0\lambda \\ + 14400C_4^{02} - 120C_4^0\lambda + \frac{25}{4}\lambda^2, \end{array}} \tag{6d}$$

$$E(^2\Sigma_{1/2}) = E_{4d} + 9/2C_2^0 + 12C_4^0 + 1/4\,\lambda - \frac{1}{2}\sqrt{\begin{array}{l} 9C_2^{02} + 720C_2^0C_4^0 - 3C_2^0\lambda \\ + 14400C_4^{02} - 120C_4^0\lambda + \frac{25}{4}\lambda^2. \end{array}} \tag{6e}$$

TABLE I

E_{4d}, C_2^0, C_4^0 and λ for Me_2Cd and Et_2Cd[a]

	Me_2Cd	Et_2Cd
C_2^0	−0.0225(8)	−0.023(2)
C_4^0	−0.0008(1)	−0.0012(4)
λ	+0.685(10)	+0.688(20)
E_{4d}	17.747	17.497

[a] Estimated error in parentheses.

With five peak positions, and five equations, the four unknowns (E_{4d}, C_2^0, C_4^0 and λ) can be readily obtained, and these are given in Table I for Me_2Cd and Et_2Cd. Using these parameters, the agreement between calculated and observed peak positions for Me_2Cd (Table II) is really quite remarkable—within 0.012 eV for all peak positions. The ordering of the energy states in Table II, $^2\Delta_{3/2} > {}^2\Pi_{1/2} > {}^2\Delta_{5/2} > {}^2\Pi_{3/2} > {}^2\Sigma_{1/2}$, is the same as that observed, $\Delta > \Pi > \Sigma$, for $CuCl_2$ without spin-orbit splitting. This sequence corresponds to the orbital energy ordering $\sigma > \pi > \delta$ which is just the order mentioned earlier for $CuCl_2$ for a purely electrostatic perturbation of the metal d orbitals. Several other comparisons between the Me_2Cd and $CuCl_2$ spectra should be made. First, the signs of C_2^0 and C_4^0 are both negative as for $CuCl_2$. This, of course, follows from the same energy ordering above. Second, the ratio of C_2^0/C_4^0 of 20 for Me_2Cd and 19 for Et_2Cd are both large and rather similar to the C_2^0/C_4^0 ratio of 30 obtained for $CuCl_2$. However, the magnitudes of C_2^0 and C_4^0 are close to an order of magnitude smaller than for $CuCl_2$ while λ for Cd^{2+} is much larger than that for Cu^{2+}. Similar results are obtained for the Zn 3d peaks in Et_2Zn (Fig. 6). The Zn ion state ($3d^9$) is isoelectronic with the Cu $3d^9$ state in $CuCl_2$.

TABLE II

One-electron eigenfunctions and energies for the Cd 4d level in Me_2Cd

Approximate M_j	Term	Eigenfunction	E (eV) Expt.	Calc.
1/2	$^2\Sigma_{1/2}$	$0.54d_\pi\beta + 0.84d_\sigma\alpha$	17.349	17.344
3/2	$^2\Pi_{3/2}$	$0.38d_\delta\beta + 0.93d_\pi\alpha$	17.483	17.475
5/2	$^2\Delta_{5/2}$	$d_\delta\alpha$	17.589	17.601
1/2	$^2\Pi_{1/2}$	$0.84d_\pi\beta - 0.54d_\sigma\alpha$	18.053	18.064
3/2	$^2\Delta_{3/2}$	$0.93d_\delta\beta - 0.38d_\pi\alpha$	18.262	18.252

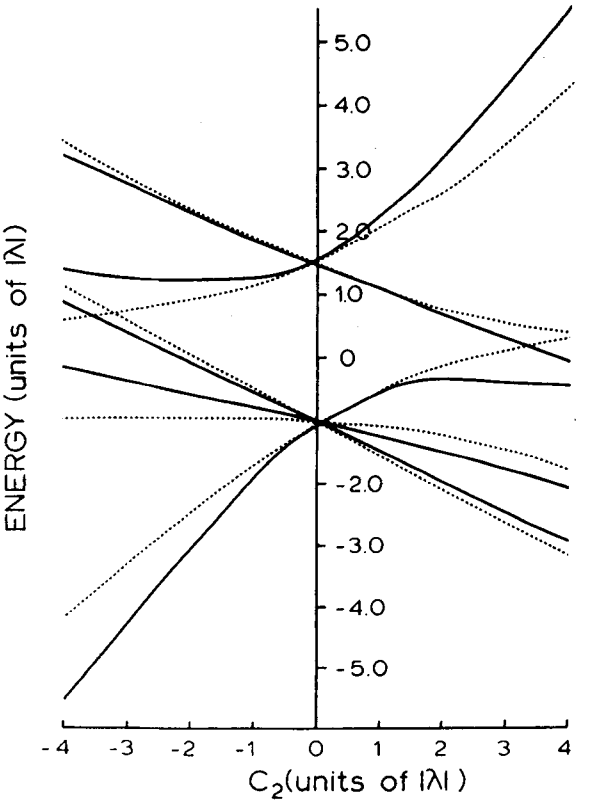

FIGURE 7 General energy-level diagram for the combined spin-orbit splitting and crystal-field interaction [see Eq. (6)] for a C_2^0/C_4^0 ratio of 20 (-----), and a C_2^0/C_4^0 ratio of 10 (——).

A general energy-level diagram is readily constructed from Eqs. (6). this is shown in Fig. 7 for two values of the C_2^0/C_4^0 ratio. Any core d spectrum observed so far can be readily related to this diagram.

High-resolution spectra of the Zn 3d and Cd 4d orbitals of the gas phase Zn and Cd halides have been obtained[10] more recently at elevated temperatures (Fig. 8). These spectra are a bit more complicated than the alkyl Zn and Cd spectra. Only five peaks are clearly discernable in ZnI_2, but additional peaks are present in $ZnBr_2$ and $ZnCl_2$. In $ZnCl_2$, the additional peaks are due to vi-

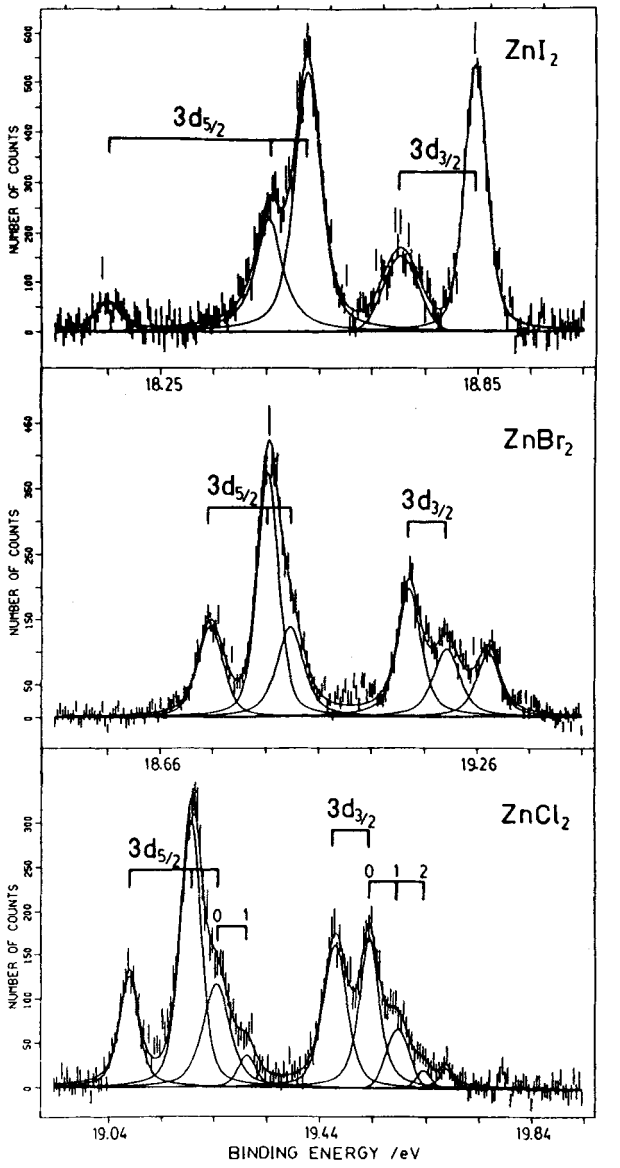

FIGURE 8 Photoelectron spectra of the Zn 3d levels in ZnI_2, $ZnBr_2$ and $ZnCl_2$ taken with HeII radiation (Ref. 10).

brational broadening, but the origin of the peak in $ZnBr_2$ at ~19.2 eV is not known.

One of the first questions which arises with these low-lying metal core d levels having a binding energy of 16–20 eV is: Are these core orbitals or do they have substantial bonding character? There are several pieces of evidence that show that these orbitals have little or no involvement in bonding. First, *ab initio* calculations on Me_2Cd[7], show that the order of one-electron metal d energies is $\sigma > \pi > \delta$ which is just that expected on the basis of a nonbonding electrostatic effect. Covalent σ bonding to the $4d_{z^2}$ orbital would, of course, lower the energy of this d_{z^2} orbital relative to the other two. Second, using the crystal-field Hamiltonian, we obtain an excellent fit to the experimental results and with a C_2^0/C_4^0 ratio which is similar to that for $CuCl_2$. Third, more detailed aspects of the spectra such as the relative linewidths and intensities are consistent with the one-electron levels given in Table II.[7] Fourth, the spin-orbit splittings observed (5/2 λ) are usually in excellent agreement with the free ion values of 0.699 for Cd^{2+} and 0.337 eV for Zn^{2+}.[15] It should also be noted here that the order of Zn 3d levels calculated from a pseudopotential calculation on Me_2Zn is $\sigma > \delta > \pi$.[30] This order reverses the δ and π orbitals from the "electrostatic order" given above, but it is more likely due to the choice of pseudopotential or basis set. In addition, for some Zn and Cd halides such as ZnI_2 and CdI_2, there is evidence that d_{z^2} is weakly involved in bonding; and in these cases, the C_2^0 parameters are calculated without using the $\Sigma_{1/2}$ energy.[10] Obviously, it would be desirable to measure these splittings on deeper core levels with larger binding energies to avoid such affects, and monochromatized synchrotron radiation will be important for obtaining crystal-field splittings on these core levels (see later section).

The C_2^0 values have been interpreted using an atomic theoretical framework.[9] The electric field which contributes to the C_2^0 term at the electronic site can be written as a sum of a term from the p valence electrons (so-called $eq_{valence}$) and a point charge crystal-field term C_2^0 ligand. Taking Me_2Zn as an example, the linear C—Zn—C linkage involves 4s and $4p_z$ Zn bonding orbitals. The dominant contribution to the observed Zn 3d C_2^0 value comes from the $eq_{valence}$ term, the electrostatic interaction between the Zn $4p_z$ electrons and the core Zn 3d orbitals. Considering this pd inter-

action, atomic F^2, G^1 and G^3 Slater–Condon integrals are of importance, but F^2 is usually dominant. We can then write:

$$eq_{\text{valence}} \propto F^2(\Delta\rho) \tag{7}$$

where $\Delta\rho = n_{p_z} - (1/2)(n_{p_x} + n_{p_y})$ [n's are the orbital populations]. For Me_2Zn, $\Delta\rho$ is very close to n_{p_z}. It should be noted that this valence term does not contribute directly to C_4^0, but C_4^0-like terms may well arise from the neglect of certain cross terms in the pd interaction.[9]

The point charge contribution can be readily calculated from crystal-field theory. For example, one point charge ($Z_q e$) a distance R from the Zn nucleus gives:

$$C_{2\ \text{ligand}}^0 = \frac{1}{21} \langle r^2 \rangle_{3d}\, Ze^2/R^3 \tag{8}$$

where $\langle r^2 \rangle_{3d}$ is the mean square radius of the Zn 3d orbital. Such point charges contribute directly to the C_4^0 term as well. The $C_{2\ \text{ligand}}^0$ term is expected to be smaller than eq_{valence} for Me_2Zn mainly because the substantial Zn $4p_z$ electron density is much closer to the Zn 3d electrons than the ligand charges. However, the C_2^0 ligand term will dominate the observed C_2^0 for more ionic compounds such as the alkali halides discussed in the next section. A simple numerical example of a C_2^0 calculation will be given in that section.

The C_2^0 values for a number of Zn, Cd, Tl, Xe, Ga and In compounds have now been derived (Table III). There are a number of interesting trends in the results, two of which are of considerable structural and bonding interest. First, $|C_2^0|$ for the Zn and Cd compounds, respectively, increase in the order Cl < Br < I < Me < Et < nPr < Me_3SiCH_2. This increase can be readily attributed to an increase in valence p_z ($4p_z$ for Zn, and $5p_z$ for Cd) electron density in the above order. This order is consistent with the accepted order of increasing donor strengths for these ligands.[33,34] There are also correlations between chemical shift and C_2^0 values[8,35] which are consistent with this order. Second, very recent gas phase studies of the indium trihalides[35] show that they give narrow fea-

TABLE III

C_2^0 values for a number of molecules[a] (eV)

Level	Geometry	Compound	C_2^0 Observed	C_2^0 Calculated	Ref
Zn 3d	linear	$ZnCl_2$	−0.0079	−0.010	10
		$ZnBr_2$	−0.0084	−0.008	10
		ZnI_2	−0.014	−0.0055	10
		Me_2Zn	−0.0169(7)		8
		Et_2Zn	−0.0175(7)		8
Cd 4d	linear	$CdCl_2$	−0.016	−0.017	10
		$CdBr_2$	−0.020	−0.012	10
		CdI_2	−0.023	−0.0089	10
		Me_2Cd	−0.0225(8)		8
		Et_2Cd	−0.023(2)		8
		$(nPr)_2Cd$	−0.025(2)		8
		$(Me_3SiCH_2)_2Cd$	−0.030(3)		8
Tl 5d	linear	TlCl	−0.0210	−0.022	11
		TlBr	−0.0233	−0.023	11
		TlI	−0.0258	−0.026	11
Xe 4d	linear	XeF_2	+0.041(4)		32
	square planar	XeF_4	−0.045(4)		32
Ga 3d	planar	Me_3Ga	+0.021(2)		31
In 4d	planar	Me_3In	+0.024(2)		29
	dimers[35]	$InBr_3$	~0.006		35
	dimers[35]	InI_3	~0.007		35

[a] Errors are usually given in brackets.

tureless In 4d spectra (Fig. 9). Previous valence-band photoelectron studies of these compounds assumed they were monomeric planar species.[36] However, by analogy with the Zn and Cd halides and alkyl compounds, we would expect monomeric InI_3 to have a similar C_2^0 to the known monomeric Me_3In (Table III). Instead, a narrow line is observed with C_2^0 at most being one-quarter of the C_2^0 for Me_3In. Our spectrum shows that InI_3 is, in fact, a pseudotetrahedral dimer which would be expected to give a very small C_2^0 value.[35] These results show the considerable potential of the ligand-field splittings to extract bonding and structural information.

Other trends are of more theoretical interest. First, the Zn compounds have substantially smaller C_2^0 values than their Cd analogues. Using Eq. (7), the lower Zn C_2^0 values are mainly due to

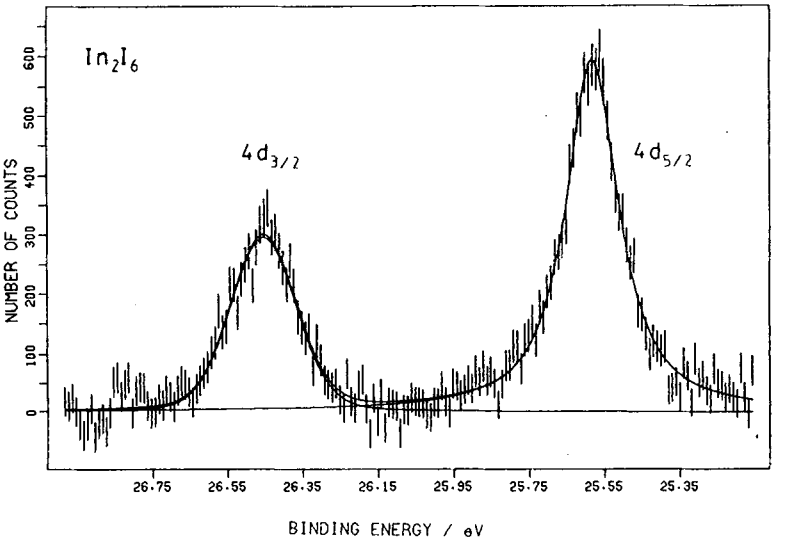

FIGURE 9 In 4d spectrum of In_2I_6 taken with HeII radiation (Ref. 35).

the lower F^2 values for Zn (0.0715 Ry) compared to Cd (0.0830 Ry). Also, the $\Delta\rho$ values for Me_2Zn and Me_2Cd from *ab initio* calculations are 0.39 and 0.43 *e*, respectively.[7,29] The ratio of $[F_2(\Delta\rho)]_{Me_2Zn}/[F^2(\Delta\rho)]_{Me_2Cd}$ becomes 0.78, and this is in excellent agreement with the experimental ratio of 0.75. A similar trend is seen for the Me_3Ga and Me_3In analogues. Second, the linear species give negative C_2^0 values, while Me_3M (M = Ga, In) have positive C_2^0 values corresponding to an excess of valence charge density in p_x and p_y. Linear XeF_2 has a positive C_2^0 because of withdrawal of $5p_z$ electron density from the Xe $5p^6$ configuration by the electronegative fluorines. The XeF_2 and XeF_4 results are consistent with the ligand-field splittings obtained using absorption spectroscopy.[37] The magnitudes of the C_2^0 values are also consistent with the nuclear field gradients discussed in a later section.

The Ga, In, Tl and Xe spectra are not as well resolved as the Zn and Cd spectra for two reasons. First, the inherent width of the d levels increases from Group IIB ($\leq$0.05 eV) to Group III ($\sim$0.15 eV) to Group IV ($\sim$0 3 eV).[9] Second, the linewidth of the x-ray source (used for the Xe spectra) was much broader than the

HeI and HeII sources. The errors in these C_2^0 values are thus larger than those for the Zn and Cd compounds. Finally, theoretical calculations of C_2^0 for the Zn halides are in at least qualitative agreement with experimental values; while for the Tl halides, there is very good agreement.

A few other papers have reported line broadenings on Group IV Sn 4d and Pb 5d levels.[38-42] This data has not been analyzed quantitatively, but the qualitative results are consistent with the above treatment. The larger inherent linewidths for the Sn 4d and Pb 5d levels will probably make it impossible to resolve splittings in compounds of these elements. If a large number of spectra are obtained to high statistics, it may still be possible to obtain semiquantitative results on Sn and Pb compounds.

LIGAND-FIELD SPLITTING ON p ORBITALS

A number of papers have reported high temperature HeI and HeII photoelectron spectra of alkali halide monomers in the gas phase.[42-49] The observed spin-orbit splitting of the halide p levels is generally substantially larger than the free ion value in contrast to the much lower value for covalently bonded halides such as HI. These alkali halide spin-orbit splittings support an ionic formalism for the monomers. In the iodides, the apparent I 5p spin-orbit splitting increases from CsI to LiI. The $5p_{3/2}$ peak is always significantly broader than the $5p_{1/2}$ peak, and in NaI and LiI, the $5p_{3/2}$ peak splits into a resolved doublet.

Based on *ab initio* M.O. calculations, Berkowitz *et al.*[43,49] were able to obtain quantitative agreement with experiment. However, these results can be explained—at least semiquantitatively—based on a pure ionic model, and this gives us an excellent opportunity to use a very simple and general calculation to explain the ligand-field splitting.

Consider, then, a purely ionic NaI molecule with the Na^+ point charge a distance 2.7115 Å[50] from the iodide ion having a $5p^6$ configuration. After photoionization of an I^- 5p electron a ^2P ion term is obtained (Fig. 10). The crystal-field potential for the Na^+ point charge is given by Eq. (1) without the Y_4^0 term which vanishes by symmetry for p electrons. Recast in the operator equivalent

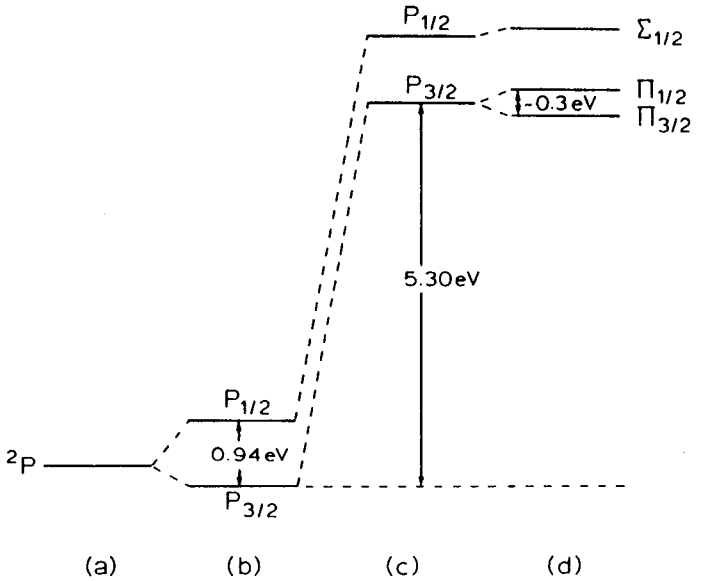

FIGURE 10 Energy-level diagram for the 5p level in Na I after photoionization of an I 5p electron: (a) the ^2P term for a "free" I^0 atom (binding energy 3.51 eV); (b) spin-orbit splitting; (c) the chemical shift from the Na^+ ion due to the A_0^0 crystal field term; (d) the crystal-field splitting from the A_2^0 or C_2^0 term.

model, the Hamiltonian becomes:

$$H = \Delta E_b + C_2^0[3L_z^2 - L(L+1)] + \lambda[(1/2)(L_+S_- + L_-S_+) + L_zS_z] \quad (9)$$

where ΔE_b is the shift of the free I^- ion 5p binding energy (3.51 eV)[51] due to the Na^+ point charge. ΔE_b is just given by Ze^2/R, $C_2^0 = 1/5\ \langle r^2\rangle_{I\,5p} Ze^2/R^3$, $\langle r^2\rangle = 7.201$ a.u.[9] and $\lambda = 0.628$ eV. We can now readily calculate complete energy-level diagrams (Figs. 10 and 11) for the I $5p^5$ ion state.

$$\Delta E_b = 1/(2.7115 \times 10^{-8}) = 3.69 \times 10^7\ \text{cm}^{-1}.$$

Multiplying by e^2 ($e = 4.80 \times 10^{-10}$ esu) gives $\Delta E_b = 8.50 \times 10^{-12}$ ergs. Since 1 erg $= 6.24 \times 10^{11}$ eV, ΔE_b becomes 5.30 eV.

This is perhaps more easily obtained using atomic units [1 a.u.(r) = 0.529 Å; 1 a.u.(E) = 27.21 eV]. Thus 2.7115 Å = 5.13 a.u. and $1/R$ = 0.195 a.u. Multiplying by 27.21 eV gives ΔE_b = 5.30 eV again. The total binding energy E_b for the I 5p electron becomes 5.30 + 3.51 = 8.81 eV, in excellent agreement with the experimental value of 8.85 eV.[44]

Now C_2^0 is just as easily calculated. Using atomic units, C_2^0 = $(0.20 \times 1 \times 7.201)/(5.13)^3$ = 0.0107 a.u. which when multiplied by 27.21 becomes 0.291 eV. To compare this calculated C_2^0, we must obtain a C_2^0 from the measured spectrum and the energy levels obtained from the Hamiltonian in Eq. (9). The energy levels are (including the binding energy):

$$E_{\Pi_{3/2}} = E_b - C_2^0 - 1/2\,\lambda \tag{10a}$$

$$E_{\Pi_{1/2}} = E_b + (1/2)\left[C_2^0 + \frac{1}{2}\lambda - \sqrt{\left[\frac{3\lambda^2}{2}\right] - 3\lambda C_2^0 + 9C_2^{02}}\right] \tag{10b}$$

$$E_{\Sigma_{1/2}} = E_b + (1/2)\left[C_2^0 + \frac{1}{2}\lambda + \sqrt{\left[\frac{3\lambda^2}{2}\right] - 3\lambda C_2^0 + 9C_2^{02}}\right] \tag{10c}$$

These energy levels are plotted in Fig. 11 for differing values of C_2^0 (in units of λ). The ^{2}P level splits into two—the $\Pi_{1/2}$ and $\Pi_{3/2}$ states. Taking the quoted peak positions given by Potts *et al.*[44] for these three levels gives $\Sigma_{1.2} - \Pi_{1/2}$ = 0.96 eV, and $\Sigma_{1/2} - \Pi_{3/2}$ = 1.18 eV. Solving for λ and C_2^0 in Eqs. (10) gives $(C_2^0)_{obs}$ = +0.13 eV and λ = 0.68 eV. Taking the possible errors into account, $(C_2^0)_{obs}$ could be as large as 0.19 eV. These values are substantially smaller than the calculated value based on a point charge. Better agreement (0.22 eV) is obtained considering Sternheimer shielding factors or covalency effects.[9]

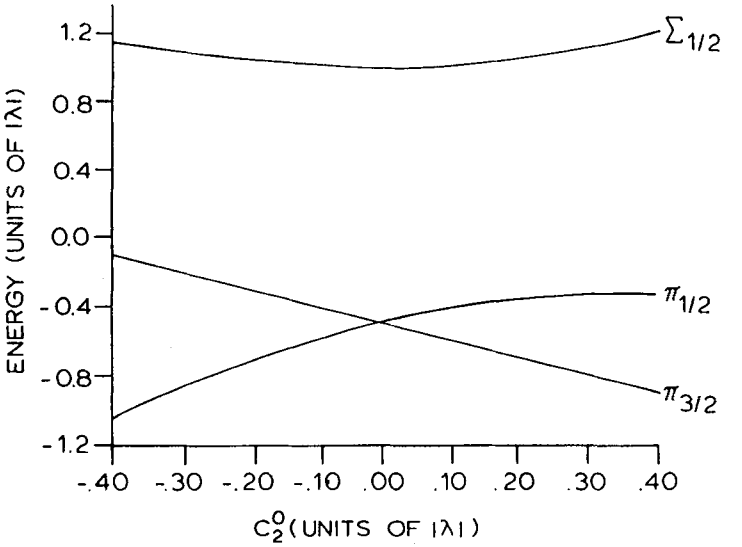

FIGURE 11 General energy-level diagram for the combined spin-orbit splitting and crystal-field interaction [see Eq. (9)].

Using the simple formula for ΔE_b and C_2^0, it is apparent the C_2^0 will increase rapidly as R decreases. Thus we would expect LiI to have the largest C_2^0 and CsI the smallest. Indeed, well-resolved $p_{3/2}$ splitting has been observed in LiI. These splittings are just as large (~0.2–0.3 eV) as those observed in the order $Cl^- < Br^- < I^-$, so that the C_2^0 values for iodides will be the largest. The linewidths so far observed for these high temperature species are much larger than those observed for the Zn and Cd compounds due mostly to vibrational broadening. If better resolution can be achieved, these splittings will be seen on many more outer halide p orbitals.[9] We have also shown that the splitting on the outer alkali metal p orbitals should be observable[9] and the left-hand side of Fig. 11 will be required for this case.

LIGAND-FIELD SPLITTING AND NUCLEAR FIELD GRADIENTS

We have noted in previous papers that the C_2^0 term ($H_{C_2^0}$) in Eqs. (2) and (9) transform like the nuclear quadrupole Hamiltonian

(neglecting the η (or C_2^2) term.[52,53]

$$H_Q = \frac{e^2 q_n Q}{4I(2I - 1)} [3I_{z^2} - I(I + 1)] \tag{11}$$

where eQ is the nuclear quadrupole moment of the nucleus, eq_n is the so-called field gradient set up by the ligands, and I and I_z are the nuclear spin momentum operators. Comparing $H_{C_2^0}$ with Eq. (11), it is immediately obvious that $C_2^0 \propto q_n$. For this reason, we initially termed the Cd and Zn d splitting, the electric field gradient splitting. However, Jorgenson pointed out that the electric field gradient could only be measured at the nucleus. However, it is the same asymmetric ligand field that is measured at the electronic site and at the nucleus, and the ligand-field splitting offers us a marvellous opportunity for observing the transmission of the ligand field through the atom to the nucleus.

Traditionally, the nuclear field gradient (eq_n) is divided up into two terms[53]:

$$eq_n = eq_{\text{valence}} (1 - R_n) + eq_{\text{ligand}} (1 - \lambda_n) \tag{12}$$

where eq_{valence} is analogous to the term in Eq. (7), eq_{ligand} is just the point charge term and λ and R are Sternheimer factors which take into account the polarization of both core and valence electrons. To a first approximation, the electric field at a core electronic site (eq_c) may be written in an analogous manner:

$$eq_c = eq_{\text{valence}} (1 - R_c) + eq_{\text{ligand}} (1 - \lambda_c) \tag{13}$$

where the eq_{valence} and eq_{ligand} are the same electric field in both Eqs. (12) and (13), but the Sternheimer factors differ. The eq_{ligand} term is usually written for the nuclear case[53]:

$$eq_{\text{ligand}} = \frac{e \sum_i Z_i (3 \cos^2\theta_i - 1)}{R_i^3} \tag{14}$$

where $(3 \cos^2\theta_i - 1)$ is just proportional to the Y_2^0 spherical harmonic. For monomeric NaBr in the gas phase $|eq_{\text{ligand}}|$ at either the Na or Br nucleus becomes $2e/R^3$. The same results is obtained

from standard crystal-field theory: $|eq_{\text{ligand}}| = \sqrt{5/\pi}|A_2^0|, |A_2^0| = 2\sqrt{\pi/5}\ Ze^2/R$, and so $|eq_{\text{ligand}}| = 2e/R^3$.

For a point charge contribution alone to both eq_n and eq_c, it is easy from Eqs. (12) and (13) to see that eq_n is related to eq_c just by the Sternheimer factors $(1 - \lambda_x)$[54]:

$$eq_n = \left[\frac{1 - \lambda_n}{1 - \lambda_c}\right] eq_c \tag{15}$$

To demonstrate the use of the above equations, we choose to calculate both eq_n and eq_c at the Br nucleus and Br 4p site, respectively, in NaBr monomer, and then see how these calculations agree with the experimental eq_n and eq_c. For these calculations, we require $(1 - \lambda_n) = 141$ and $(1 - \lambda_c) = 0.57$,[55] $\langle r^3 \rangle_{\text{Br}} = 5.224$ a.u.[9] and $R_{\text{NaBr}} = 2.502$ Å.[50] eq_{ligand} for the Na^+ at Br^- is $9.60 \times 10^{-10}/(2.50 \times 10^{-8})^3 = 6.15 \times 10^{13}$ esu cm^{-3}. Multiplying by $(1 - \lambda_c)$ gives $eq_c = 3.51 \times 10^{13}$ esu cm^{-3}. From Eq. (15), eq_n becomes 8.68×10^{15} esu cm^{-3}, two orders of magnitude larger than eq_c. eq_n agrees qualitatively with the measured 2.58×10^{15} esu cm^{-3}.[52] C_2^0 at the Br 4p site can be readily calculated from an expression analogous to that given earlier for d electrons [Eq. (8)]:

$$C_2^0 = 1/5\ \langle r^2 \rangle_{\text{Br,4p}} Ze^2/R^3(1 - \lambda_c) \tag{16a}$$

$$= 1/10\ \langle r^2 \rangle_{\text{Br,4p}}\ e^2 q_c \tag{16b}$$

Substituting gives $C_2^0 = 0.1 \times (1.46 \times 10^{-16}) \times 4.80 \times 10^{-10} \times 3.51 \times 10^{-13} = 2.46 \times 10^{-13}$ ergs $= 0.15$ eV. This C_2^0 enables the Br 4p photoelectron spectrum to be fitted adequately and is close to the value obtained for NaI earlier. The reasonable agreement for both eq_c and eq_n based on this simple point charge model is very encouraging, and shows that indeed it is possible to obtain eq_n from eq_c or vice versa to within at least a factor of 3 or 4.

For covalent molecules, we can calculate $\Delta\rho$ and eq_{valence} at both sites. Because $C_2^0 \propto F^2\ \Delta\rho$ [Eq. (7)], it is possible to calculate $\Delta\rho$ from the measured C_2^0 value, and then use the standard equation:

$$eq_{\text{valence}} = 4/5\ e\langle r^{-3} \rangle \Delta\rho \tag{17}$$

for calculating eq_{valence} at the nuclear site. Nuclear field gradients calculated in this way are in good agreement with the experimental results obtained from Mössbauer spectroscopy, nuclear quadrupole resonance (NQR) and perturbed angular correlation (PAC). The derived eq_n results have also been used to test the accuracy of nuclear quadrupole moments eQ.[55]

Finally, it is worth emphasizing that for analogous ionic molecules (e.g., NaCl and NaBr) or analogous covalent molecules (e.g., Me_2Cd, Me_2Zn, Me_3Ga), there is a good correlation between eq_c and eq_n. Thus eq_n values from Mössbauer, NQR or PAC measurements can be used as an excellent guide in looking for molecules with large and measureable eq_c. For example, Me_3SnCl has a large eq_n at the Sn nucleus[53] and therefore must have a C_2^0 value comparable to or larger than C_2^0 for Me_2Cd. The ligand-field splittings of ~0.25 eV are difficult to observe because the Sn 4d lines are broad (~0.3 eV).

FUTURE DEVELOPMENTS

In the near future, two developments will enable ligand-field splittings to be observed on a large number of compounds of many elements. First, high temperature inlet systems have enabled, and will enable, more involatile compounds to be run in the gas phase. Second, synchrotron radiation provides[20] a narrow line photon source to $\geq$100 eV, and will enable many more energy levels to be probed at the required high resolution, both in the gas and solid state.

Many of the spectra described in this Comment have been obtained using high temperature inlets. The alkali halides are especially notable in this regard. In the near future, many more involatile inorganic and organometallic compounds of Zn, Cd, Ga, In, Tl and the alkalis could be easily obtained in the gas phase using existing HeI and HeII sources. Such studies should have interesting bonding and structural uses. For example, the Zn 3d and Cd 4d spectra of Zn and Cd porphyrin compounds should provide very useful insights into the bonding in these compounds. On the structural side, core-level splittings should be useful in

measuring monomer–dimer equilibria in Group III Al, Ga and In compounds, as has already been shown for the indium trihalides.[35]

The use of synchrotron radiation will have a much greater impact on photoelectron spectra in general, and the development of this ligand-field splitting area in particular. The greatest restriction to observing ligand-field splittings in many elements at the present time is due to poor resolution at photon energies above 40.8 eV. As we have shown in Fig. 6, the splittings are normally in the 0.2–0.3 eV range, and high resolution is obviously required.

What are the contributions to the total observed linewidth Γ_{total}? For gases, Γ_{total} can be expressed roughly by[56,57]:

$$\Gamma_{total} \sim \Gamma_{source} + \Gamma_{analyzer} + \Gamma_{line} \tag{18}$$

where Γ_{source} is the linewidth of the exciting radiation (~0.7 eV for Mg $K\alpha$ and ~1 meV for HeI), $\Gamma_{analyzer}$ is the linewidth contribution due to the analyzer, lens and slit resolution, and Γ_{line} is the inherent lifetime Heisenburg width. As indicated above, Γ_{source} for He radiation is small, while that for x rays is very large, thus leading to the dramatic difference in resolution of the two spectra in Fig. 5. $\Gamma_{analyzer}$ is usually less than 0.1 eV and Γ_{line} is often very small, <0.3 eV for many low lying core levels. For example, in Table IV, we list narrow core levels, many of which have $\Gamma_{line} \leq 0.1$ eV.

TABLE IV

Narrow, low binding energy, levels of chemical interest (Ref. 9)

Element and Energy Level	Number of Elements	Approximate Binding Energy (eV)
Li 1s → C 1s	4	55–290
Na 2p → S 2p	6	30–165
Cl 3p → Ti 3p	6	10– 34
Zn 3d → Kr 3d	7	16– 90
Rb 4p → Zr 4p	4	20– 35
Cd 4d → Xe 4d	7	16– 75
Cs 5p → Ce 5p	4	12– 25
Hf 4f → Au 4f	8	20– 75
Hg 5d → Pb 5d	3	15– 25
Th 6p, U 6p	2	20

It should also be noted that other effects such as charge broadening can be important for gas phase compounds, and even more important for some solids. The gas phase charging problem can usually be minimized so that linewidths of ≤50 meV can be obtained on organometallics (Fig. 6) compared to ~20 meV for Ar (Fig. 5). However, nonconductor solid state linewidths are at least 0.15 eV larger than gas, metal and semiconductor linewidths.[38] For this reason alone, resolved ligand-field splittings will probably not be observed using nonconductor solids, but could be resolved on metal and semiconductor surfaces.

From the above discussion, it is apparent that Γ_{total} can approach 0.1 eV for narrow lines and high instrumental resolution if Γ_{source} is ≤0.1 eV. The highest energy sources now routinely used are the HeII lines at 40.8 eV, 48.4 eV, 51.2 eV and 52.0 eV. In practice, it is very difficult to obtain core-level spectra above E_b ~ 30 eV because the higher energy HeII lines are very weak, and all the spectra overlap. It has already been shown that mono-

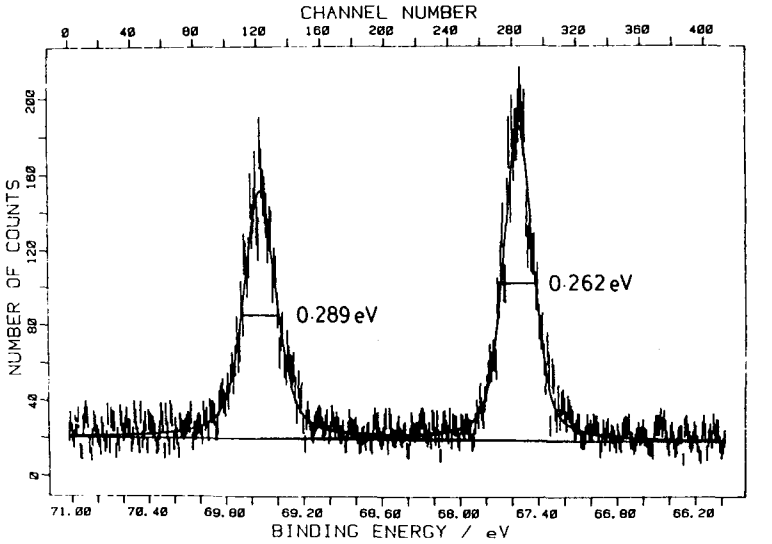

FIGURE 12 Xe 4d photoelectron spectrum of Xe gas taken with 94 eV photon energies using monochromatized synchrotron radiation (Ref. 20).

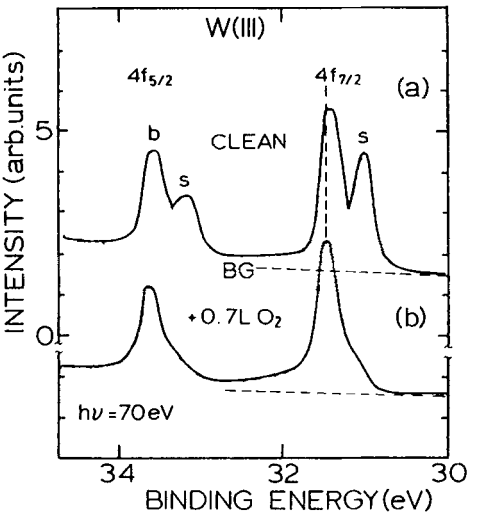

FIGURE 13 High-resolution spectrum of a clean W(III) surface taken with monochromatized synchrotron radiation at 70 eV (Ref. 61). W 4f peaks due to the bulk (b) and surface (s) atoms are denoted in the upper spectrum.

chromatized synchrotron radiation will yield narrow lines above 100 eV (Refs. 19–21, and references therein). For example, we have already obtained Xe 4d linewidths of 0.26 eV (Fig. 12) at photon energies of 94 eV.[20] Monochromatized Al $K\alpha$ radiation[58,59] yields similar widths. Such sources should open up high resolution possibilities for many of the 5l core levels listed in Table IV, and enable resolution of ligand-field splittings on compounds of elements such as Xe and Si. Indeed, the monochromatized sources have already resolved the surface layer from the bulk in metals such as W, Ir and Au (Fig. 13) and semiconductors such as GaAs.[21,60,61] The low symmetry surface atoms have broader linewidths than the bulk atoms, and this broadening has been attributed to unresolved crystal-field splitting.[21] Although it seems unlikely that the surface splitting will be resolved, the crystal-field broadening should be useful for distinguishing and characterizing the symmetry of surface atoms, especially after adsorption of small molecules onto the surface layer.

Acknowledgments

Our studies have been supported by the Natural Sciences and Engineering Research Council of Canada, and the University of Western Ontario. We wish to acknowledge the valuable experimental and theoretical contributions of our colleagues D. K. Creber, R. P. Gupta, L. L. Coatsworth, E. Pellach, R. Lazier, D. J. Bristow, J. Forrest, B. W. Yates and K. H. Tan.

G. M. BANCROFT*
Department of Chemistry,
Centre for Chemical Physics,
University of Western Ontario,
London, Ontario, Canada N6A 5B7

J. S. TSE
Chemistry Division,
National Research Council,†
Ottawa, Ontario, Canada K1A 0R9

References

1. J. Becquerel, Z. Phys. **58**, 205 (1929).
2. H. Bethe, Ann. Phys. [5]**3**, 133 (1929).
3. C. K. Jorgensen, *Absorption Spectra and Chemical Bonding in Complexes* (Pergamon, 1962).
4. C. K. Jorgensen, *Modern Aspects of Ligand Field Theory* (North-Holland, Amsterdam, 1971).
5. C. J. Ballhausen, *Introduction to Ligand Field Theory* (McGraw-Hill, New York, 1962).
6. F. A. Cotton and G. Wilkinson, *Advanced Inorganic Chemistry*, Third Edition (Interscience, 1972).
7. G. M. Bancroft, D. K. Creber and H. Basch, J. Chem. Phys. **67**, 4891 (1977).
8. D. K. Creber and G. M. Bancroft, Inorg. Chem. **19**, 643 (1980) and references.
9. R. P. Gupta, J. S. Tse and G. M. Bancroft, Philos. Trans. Roy. Soc. **293**, 535 (1980).
10. G. M. Bancroft, D. J. Bristow and J. S. Tse, Chem. Phys. **75**, 277 (1983).
11. G. M. Bancroft and D. J. Bristow, Can. J. Chem. **61**, 2669 (1983).
12. R. G. Edgell, in *Electronic Structure and Magnetism of Inorganic Compounds*, The Royal Society of Chemistry, London, 1, 117–120 (1982).
13. J. T. Hougen, G. E. Leroi and T. C. James, J. Chem. Phys. **34**, 1670 (1961).

---

*To whom correspondence should be addressed.
†Published as NRCC 24654.

14. B. Bleaney and K. W. H. Stevens, Report Prog. Phys. **16**, 108 (1953).
15. C. E. Moore, National Bureau of Standards Circ. 467 (1958).
16. T. E. Carlson, *Photoelectron and Auger Spectroscopy* (Plenum, 1975).
17. D. W. Turner, A. D. Baker, C. Baker and C. R. Brundle, *Molecular Photoelectron Spectroscopy* (Wiley, 1970).
18. K. Siegbahn *et al.*, *ESCA Applied to Free Molecules* (North Holland, 1969).
19. M. O. Krause, in *Synchrotron Radiation Research*, eds. H. Winick and S. Doniach (Plenum, New York, 1980), p. 101.
20. B. W. Yates, K. H. Tan, L. L. Coatsworth and G. M. Bancroft, Phys. Rev. A **31**, 1529 (1985).
21. G. K. Werthum, P. H. Citrin and J. F. van der Veen, Phys. Rev. B **30**, 4343 (1984) and references.
22. T. Koopmans, Physica **1**, 104 (1934).
23. R. P. Gupta and S. K. Sen, *Electron Emission Spectroscopy*, eds. W. Dekeyser *et al.* (Reidel, Holland, 1973), p. 225.
24. R. P. Gupta and S. K. Sen, Phys. Rev. Lett. **28**, 1311 (1972).
25. G. M. Bancroft, I. Adams, H. Lampe and T. K. Sham, Chem. Phys. Lett. **32**, 173 (1975).
26. J. D. H. Eland, Int. J. Mass Spect. Ion Phys. **4**, 37 (1970).
27. A. F. Orchard and N. V. Richardson, J. Elect. Spectrosc. Relat. Phen. **6**, 61 (1975).
28. G. M. Bancroft, I. Adams, D. K. Creber, D. E. Eastman and W. Gudat, Chem. Phys. Lett. **38**, 83 (1976).
29. G. M. Bancroft, L. L. Coatsworth, D. K. Creber and J. S. Tse, Phys. Scripta **16**, 217 (1977).
30. G. M. Bancroft, D. K. Creber, M. A. Ratner, J. W. Moskowitz and S. Topiol, Chem. Phys. Lett. **50**, 233 (1977).
31. G. M. Bancroft, L. L. Coatsworth, D. K. Creber and J. S. Tse, Chem. Phys. Lett. **50**, 228 (1977).
32. G. M. Bancroft, P. A. Malmquist, S. Svensson, E. Basilier, U. Gelius and K. Siegbahn, Inorg. Chem. **17**, 1595 (1978).
33. J. Shorter, Rev. Chem. Soc. **24**, 433 (1970).
34. S. Evans, J. C. Green and S. E. Jackson, J. Chem. Soc., Faraday Tras. **2**, 191 (1973).
35. J. E. Forrest, G. M. Bancroft and L. L. Coatsworth, Inorg. Chem. (in press).
36. J. L. Dehmer, J. Berkowitz, L. C. Cusachs and H. S. Aldrich, J. Chem. Phys. **61**, 594 (1974).
37. F. R. Comes, R. Haensel, U. Nielsen and W. A. E. Schwartz, J. Chem. Phys. **50**, 516 (1973).
38. G. M. Bancroft, T. K. Sham, D. E. Eastman and W. Gudat, J. Am. Chem. Soc. **99**, 1752 (1977).
39. R. G. Egdell, I. L. Fragala and A. F. Orchard, J. Elect. Spect. Rel. Phen. **17**, 267 (1979).
40. I. Fragala, E. Ciliberto, R. G. Egdell and G. Granozzi, J. Chem. Soc., Dalton Trans. 145 (1980).
41. G. M. Bancroft, E. Pellach, J. E. Forrest and J. S. Tse, unpublished results.
42. A. W. Potts and W. C. Price, Phys. Scripta **16**, 191 (1973).
43. J. Berkowitz, J. L. Dehmer and T. E. H. Walker, J. Chem. Phys. **59**, 3645 (1973).
44. A. W. Potts, T. A. Williams and W. C. Price, Proc. Roy. Soc. (London) A **341**, 147 (1974).

45. A. W. Potts and T. A. Williams, J. Chem. Soc., Faraday Trans. 2, **72**, 1892 (1976).
46. A. W. Potts and T. A. Williams, J. Chem. Soc., Faraday Trans. 1, 1892 (1977).
47. A. W. Potts and E. P. F. Lee, J. Chem. Soc., Faraday Trans. 2, 941 (1979).
48. J. Berkowitz, C. H. Batson and G. L. Goodman, J. Chem. Phys. **71**, 2624 (1979).
49. J. Berkowitz, J. L. Dehmer and T. E. H. Walker, J. Elect. Spect. Relat. Phen. **3**, 323 (1973).
50. A. Honig, M. Mandel, M. L. Stick and C. H. Townes, Phys. Rev. **96**, 629 (1954).
51. C. K. Jorgensen, *Structure and Bonding*, Vol. 24, ed. J. D. Dunitz *et al.* (Springer-Verlag, 1975).
52. E. A. C. Lucken, *Nuclear Quadrupole Coupling Constants* (Academic, New York, 1969).
53. G. M. Bancroft, *Mossbauer Spectroscopy: An Introduction for Inorganic Chemists and Geochemists* (McGraw-Hill, London, 1973).
54. R. P. Gupta, J. S. Tse and G. M. Bancroft, J. Chem. Phys. **68**, 4192 (1978).
55. T. K. Sham, J. Chem. Phys. **71**, 3744 (1979).
56. K. D. Sevier, *Low Energy Electron Spectroscopy* (Wiley–Interscience, New York, 1972).
57. G. M. Bancroft, W. Gudat and D. E. Eastman, J. Elect. Spect. **10**, 407 (1977).
58. U. Gelius, S. Svensson, H. Siegbahn, E. Basilier, A. Faxlav and K. Siegbahn, Chem. Phys. Lett. **28**, 1 (1974).
59. U. Gelius, L. Asplund, E. Basilier, S. Hadman, K. Helenelund and K. Siegbahn, Nucl. Inst. Meth. **229**, 85 (1984).
60. J. F. van der Veen, F. J. Himpsel and D. E. Eastman, Phys. Rev. Lett. **44**, 189 (1980); Phys. Rev. **25**, 7388 (1982).
61. T. M. Duc, G. Guillot, Y. Lassailly, J. Lecante, Y. Jugnet and J. C. Vedrine, Phys. Rev. Lett. **43**, 789 (1979).